*Journal of New Materials for Electrochemical Systems 14, 197-202 (2011)*


# Electrochemical Corrosion of Al-Li-Sn Alloy in Water for Portable Hydrogen Sources Effect of Aluminum

Shu Liu, Mei-qiang Fan*, Da Chen and Chun-Ju LV

Department of Material Science and Engineering, China Jiliang University Hangzhou 310018, P. R. China

Received: April 11, 2011, Accepted: May 05, 2011, Available online: May 16, 2011

***Abstract**: The hydrogen generation of milled Al−Li−Sn alloy in water as a portable hydrogen source was examined in the current study. The optimized alloy composition presented significant improvement in terms of hydrogen generation rate and amount, with their values respectively reaching 1137 mL $g^{-1}$ $min^{-1}$ and 1147 mL $g^{-1}$ with an increase in Li/Sn weight ratio from 1:7 to 1:1. The efficiency of the alloy composition increased up to 99% with approximately 3.4 wt% hydrogen storage amount obtained. The XRD results indicated that the improved aluminum hydrolysis properties were attributed to the formation of the Li−Sn alloy, especially to the complex intermetallic compound $Li_{13}Sn_5$ produced with an increase in Li/Sn weight ratio. The Li−Sn alloy referred to an active site that acted as the initial hydrolysis center, and its hydrolysis byproduct, LiOH, can further stimulate the hydrolysis of the Al−Sn alloy.*

*Keywords: A. Aluminum alloy, Lithium, Tin; B. Hydrogen generation; C. Ball-milling*

## 1. INTRODUCTION

The use of hydrogen fuel cells is a promising move in the drive to address air pollution and the energy crisis. Hydrogen fuel cells are efficient power generators in which hydrogen energy is converted directly to electrical energy with lower $CO_2$ emission. Therefore, they are potential energy sources for mobile applications and vehicles, among others. However, their large-scale utilization is limited by the absence of efficient, cheap, and safe hydrogen storage materials that can be practically applied.

Portable hydrogen generation may be a good way to address the problem of hydrogen storage because in this process, hydrogen can be generated and supplied for fuel cells immediately where and when it is needed. Some materials such as chemical hydrides, methanol, and metals [1–3] are considered potential portable hydrogen sources due to their high hydrogen generation capacity [4–6], and in fact, a number of hydrogen generation technologies have been explored in the past. Compared with chemical hydrides and methanol, Al and Al alloys have a number of advantages such as their low cost and absence of harmful gas byproducts. For example, the cost of hydrogen generation from Al or Al alloys for supplying fuel cells is nearly 15 times lower than that of chemical hydrides such as sodium borohydride [7, 8]. Only hydrogen gas with water vapor is produced in Al hydrolysis, and the hydrolysis process can occur at 298 K. In comparison, hydrogen generation from methanol reforming has to be done at temperatures above 473 K, and the carbon monoxide present in the generated hydrogen gas is harmful to the fuel cell.

Generally, Al has to react with water under the catalytic effect of alkaline because a dense oxide layer on the Al surface prevents sustained aluminumAl hydrolysis. However, a strong alkaline solution is generally not recommended for handling due to safety concerns.

At present, there are several methods used to obtain hydrogen from Al hydrolysis in pure water or neutral aqueous solutions. Kravchenko et al. [9] found that Al alloys with zinc, tin, gallium, and indium have high reactivity, and they react with water to generate 1060 mL $g^{-1}$ hydrogen at moderate temperature. Some Other studies [10–11] found that milled Al with water-soluble inorganic salts has good hydrogen generation, with 100% efficiency and rapid hydrolysis kinetics in hot water. However, the addition of these dopants decreases the gravimetric hydrogen generation amount because they cannot react with water.

Recently, the Al−Li alloy has been reported to have a higher theoretic value of hydrogen generation than pure Al [12–13]. A low lithium content of the Al−Li alloy results in a low hydrogen yield, whereas a high lithium content may lead to uncontrollable hydrogen generation.

*To whom correspondence should be addressed: Email: fanmeiqiang@126.com
Phone: +86-571-86835738, Fax. +86-571-86835740

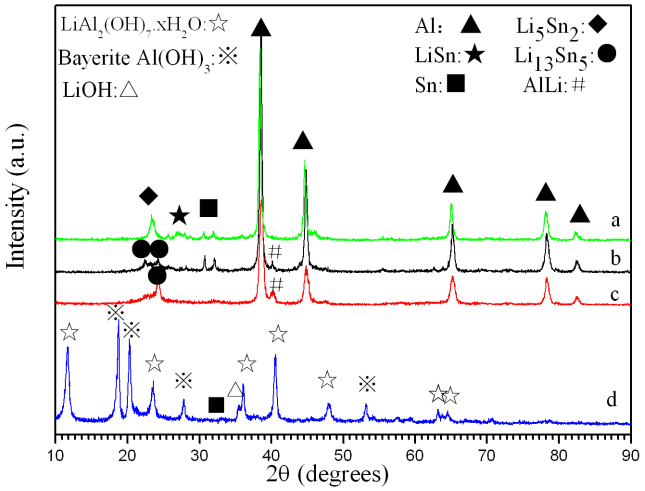


Figure 1. XRD patterns of the different aluminum alloys and their hydrolysis byproduct. a: Al−2 wt% Li−14 wt% Sn alloy, b: Al−4 wt% Li−12 wt% Sn alloy, c: Al−8 wt% Li−8 wt% Sn alloy, d: hydrolysis byproduct of Al−8 wt%, Li−8 wt%, and Sn alloy.

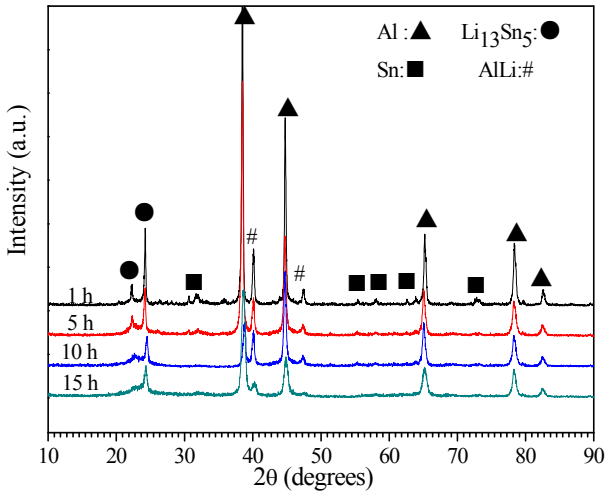


Figure 2. XRD patterns of the Al−8 wt% Li−8 wt% Sn alloy with a different milling time

The method presented in the current study is based on the milling of Al powder together with the metals Li and Sn, as well as the formation of the Al−Li−Sn alloy which has been rarely examined. The aim of the present work is to improve the amount of generated hydrogen, determine the controllable hydrogen generation rate of the aluminum alloy, explore the additive effect of aluminum reactivity according to practical needs, and optimize alloy composition.

## 2. EXPERIMENTAL

Aluminum powder (mean size, 10$\mu m$, common grade) (supplied by Beijing Xingry Technology Company Ltd.), Li flakes ( $\phi$16×0.5mm, 99.9% purity), and Sn powder (−250 mesh, 99.9% purity) (supplied by Tianjin Delan Chemical Company) were used as the starting materials. All reagents were used as received. The reagents were mixed and placed in 50 mL stainless steel jars with stainless steel milling balls set in an argon-filled glove box. The alloys were milled for 15 h in a QM−3SPO4 planetary ball miller at 450 r $min^{-1}$ under 0.2 MPa argon atmosphere.

The hydrolysis reaction was carried out at 298 K and 1 atm. The weight of the aluminum alloy was 0.2 g, and the volume of pure water was 50 mL. The aluminum alloys were thrown in water, and the produced gas was flowed through a condenser prior to measurement of hydrogen volume. The produced hydrogen volume was measured by monitoring the water displaced from a graduated cylinder as the reaction proceeded, as reported in a previous study [9]. The reaction time was calculated with the first bubble, and the final volume of the produced hydrogen was collected within 1 h of the reaction. The powder X-ray diffraction patterns (XRD) of the as-prepared samples were collected by an X-ray diffractometer (RIGAKU, Japan, model D/MAX2550V/PC). Scanning electron microscopy observations were performed using JSM−5610LV from JEOL Company, which was equipped with INCA energy dispersive X-ray spectroscopy measurements (EDS).

## 3. RESULTS AND DISCUSSION

### 3.1. Microstructure of the aluminum alloy

Fig.1 shows the X-ray diffraction patterns of the Al−Li−Sn alloy with different Li/Sn weight ratios. The peaks of $Li_5Sn_2$, LiSn, Sn, and Al are identified in the XRD patterns of the milled aluminum alloy with a Li/Sn weight ratio of 1:7. The formation of $Li_xSn_y$ alloys took place prior to that of the Al−Li alloy in the milling process; the same phenomenon has been reported in previous studies [12, 14]. With an increase in the Li/Sn weight ratio to 1:3, the new peaks of $Li_{13}Sn_5$ and Al−Li replaced those of $Li_5Sn_2$, and LiSn was obtained in the milling process. This result indicates that the higher complex compound of $Li_{13}Sn_5$ was formed from the combination of simple compounds (LiSn or $Li_5Sn_2$) and excess Li.

Excess Li metal also combined with Al to form the Al−Li alloy. However, with a further increase in the Li/Sn weight ratio up to 1:1, no new peaks appeared. Instead, the diffraction peaks of the composite became much weaker and wider, showing the gradual reduction of crystallite size and the accumulation of microstrains with a larger Li/Sn weight ratio.

Fig. 2 shows the X-ray diffraction patterns of the Al−Li−Sn alloy with different milling times. The broadened peaks show the decrease in grain size and the introduction of lattice strains during intensified milling, resulting in the uniform mixing of Li, Al, and Sn metals. From the peaks of the original Sn, Al metal, and the new $Li_{13}Sn_5$, Al−Li is indentified in the XRD patterns of the 1 h-milled Al−Li−Sn alloy.

When the milling time was prolonged to 15 h, the peaks of the Sn metal and Al−Li became wider and gradually disappeared with the formation of $Li_{13}Sn_5$, which gained Li atoms from the Al−Li alloy. Combined with Fig. 1 and 2, So This means that the existence of the AlLiAl−Li alloy depends on the Li/Sn weight ratio and the uniform mixing of Li and Sn in during the milling process-milling time.

Fig. 3 shows the morphologies of the Al−Li−Sn alloy with different milling times. A longer milling time results in a deformed morphology and decreased particle size of the powder due to cold

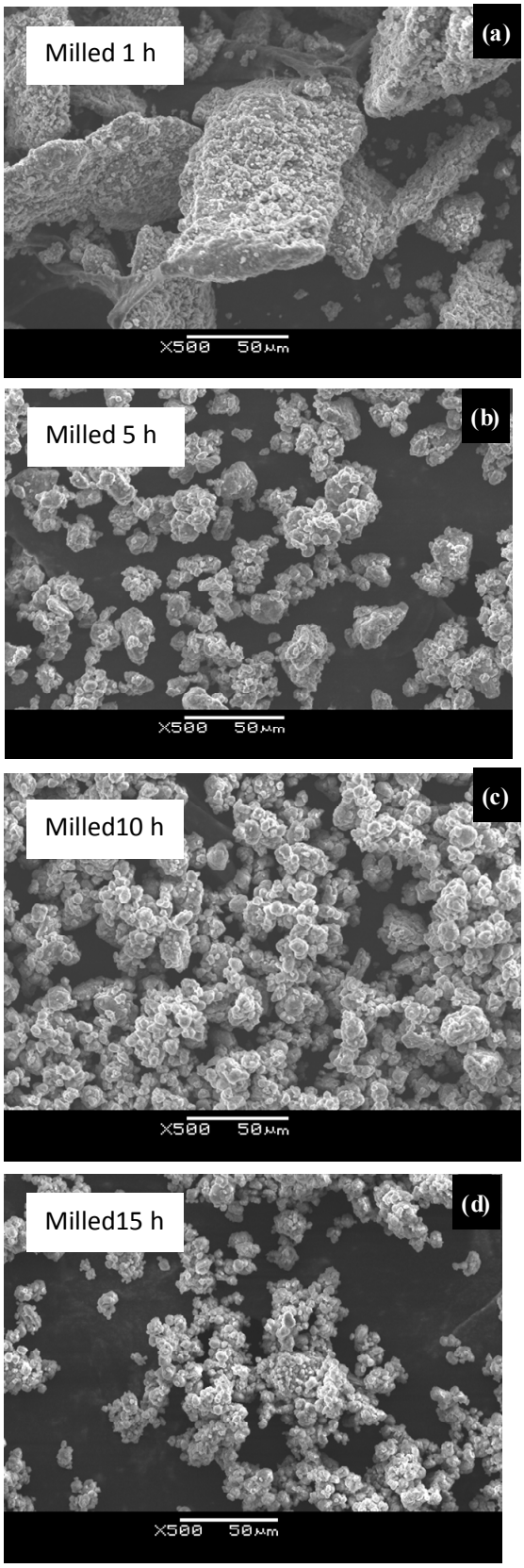


Figure 3. SEM micrographs of the Al−8 wt% Li−8 wt% Sn alloy with a different ball-milling time. (a) 1 h, (b) 5 h, (c) 10 h, (d) 15 h.

welding and repeated fracturing during the milling process. More and more irregular-shaped, small particles are obtained when the milling time is increased from 1 to 15 h. The average particle size is approximately reduced from several tenths of a micrometer to several micrometer. Therefore, a The larger surface area and a more uniform composition distribution obtained with a longer milling time are help in the complete formation of helpful to in forming new compounds completely and in improve improving hydrolysis the hydrolyticsis properties of the milled alloy.

### 3.2. Effect of the Li-Sn intermetallic compound on the hydrolysis mechanism of aluminum corrosion in water

The electrochemical corrosion of metals is constituted by anodic and catholdic reaction, occurring simultaneously on the metal surface, followed by the action of local cells [15]. In the present work, in order to determine the mechanism underlying the corrosion of the aluminum alloy, examining what reactions took place, identifying their order, and determining which of them prevails in the entire electrochemical corrosion process are necessary.

In our previous work, there was a micro-galvanic cell between Al (anode) and Sn (cathode) that stimulated hydrogen generation via the hydrolysis reaction of aluminum and water [16]. However, the addition of Li in the aluminum alloy may change the above hydrolysis mechanism of the Al−Sn alloy and water to some degree. Li−Sn alloy (including $Li_{13}Sn_5$, $Li_5Sn_2$, and LiSn) is known to have a standard potential of -2.906 V, which is lower than the -1.526 V and -1.29 V potentials of the Al−Sn alloy and of water decomposition [17], respectively. The compound $Li_{13}Sn_5$ acts as the initial hydrolysis center and reacts with water, not the Al−Sn alloy. The hydrolysis reaction is described as Reaction (1).

The hydrolysis byproduct of LiOH and Sn can further accelerate aluminum corrosion in water as the Sn distributed in the aluminum matrix [18–19] acted as the cathodic center to accelerate aluminum corrosion in the LiOH solution.

Apparent differences exist in the hydrolysis byproducts of the Al−Li−Sn and Al−Sn alloys. The XRD patterns of the hydrolysis byproducts of the Al−Li−Sn alloy are shown in Fig. 1. The peaks of $LiAl_2(OH)_7{\cdot}2H_2O$, Sn, and $Al(OH)_3$ (bayerite) are identified without AlOOH (Boehmite) [20]. Despic [21] found that Al combines easily with $OH^-$ and produces AlOH in the Al–Sn alloy hydrolysis process, as seen in Reactions 2 and 3.

AlOH is unstable and further reacted with $OH^-$ to produce $Al(OH)_3$ in the alkaline solution [22], as seen in Reaction 4. Therefore, there is a catalytic effect of the byproducts LiOH and Sn. As metal (Al or Li) hydrolysis is an exothermic reaction, a number of heat and protons are produced. These features can promote the hydrolysis rate. After aluminum corrosion, the hydrolysis byproduct $Al(OH)_3$ combines with LiOH and $H_2O$ to produce $LiAl_2(OH)_7$ hydrate in Reaction 5.

$$Li-Sn \quad + \quad OH^- + e \rightarrow LiOH + Sn \tag{1}$$

$$Al(Sn) + OH^- \rightarrow AlOH + e + Sn \tag{2}$$

$$H^+(Sn) + e \rightarrow \frac{1}{2}H_2 + Sn \tag{3}$$

$$AlOH + 2OH^- \rightarrow Al(OH)_3 + 2e \quad (4)$$

$$LiOH + 2Al(OH)_3 + 2H_2O \rightarrow LiAl_2(OH)_7.2H_2O \quad (5)$$

Fig. 4 shows the EDS mapping of the Al−8 wt% Li−8 wt% Sn alloy. The micro $Li_{13}Sn_5$ (confirmed in Fig. 1) grain is uniformly distributed in the aluminum surface and forms potential active centers with aluminum which are responsible for improving aluminum corrosion in water. The $Li_{13}Sn_5$−Al active site is very important in the formation of a micro-galvanic cell in the connection of Li−Sn, Li−Al, and Sn−Al, which have lower standard potentials compared with water decomposition. The roles of Li and Sn can be explained from the formation of active metallic compounds centered on the aluminum surface, and some compounds such as LiSn, $Li_5Sn_2$, and $Li_{13}Sn_5$, are produced with an increase in Li/Sn weight ratio. These compounds act as the initial hydrolysis center, with the high LiOH concentration and heat produced in the micro area simulating aluminum corrosion rapidly.

### 3.3. Optimized composition, preparation technology, and hydrolysis conditions of the aluminum alloy

Table 1 shows the hydrogen generation volume and maximum rate of the aluminum alloys. The aluminum alloy with a Li/Sn weight ratio of 1:7 has a higher hydrogen generation amount and rate than that in our previous work [23]. With an increase in Li/Sn weight ratio from 1:7 to 1:1, the hydrogen generation volume increases from 1,000 to 1,147 mL $g^{-1}$, and the maximum generation rate increases from 746 to 1,137 mL $g^{-1}$ $min^{-1}$. In addition, the efficiency value of hydrogen generation in the first 6 min of hydrolysis increases from 67% to 86%, with the total efficiencies exceeding 90%. The aluminum alloy with a Li/Sn weight ratio of 1:1 has the largest efficiency of up to 99%, and its hydrogen generation value reaches 3.4 wt% $\left(Hwt\% = \frac{m_H}{m_{Al} + m_{H_2O}} \times 100\%\right)$. However, when the Li/Sn weight ratio is further increased from 1:1 to 3:1, the total hydrogen generation amount decreases from 1, 147, 1070, and 1025 mL $g^{-1}$. Therefore, there is an optimized Li/Sn weight ratio at which aluminum hydrolysis properties, including hydrogen genera-

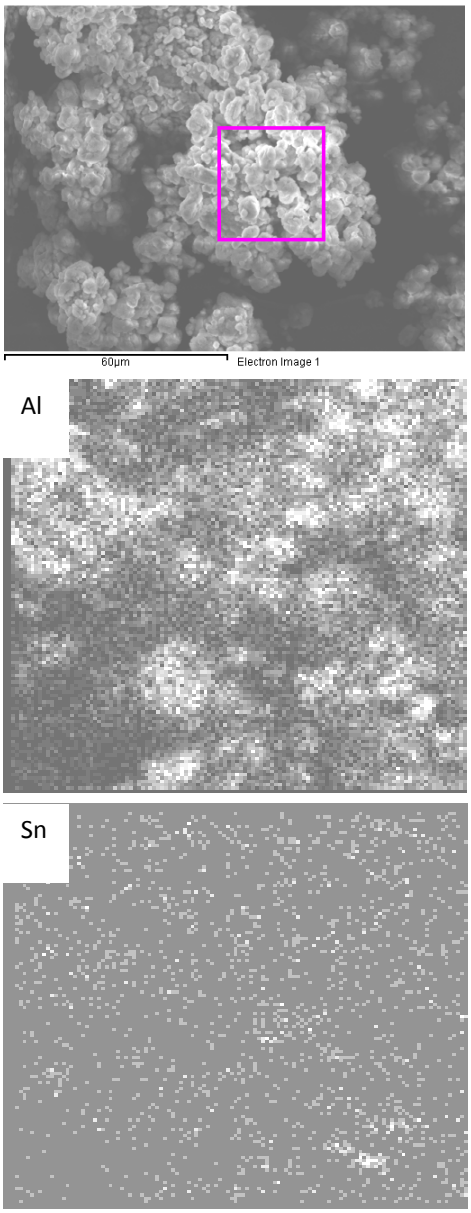


Figure 4. EDS mapping of the Al−8 wt% Li−8 wt% Sn alloy.

Table 1. Hydrogen generation volume and maximum rate of aluminum alloys (ball-milling time 15 h, $m_{water}$ /$m_{alloy}$=500, $T_{room}$=298 K)

| Alloy composition (wt%) | | | Maximum hydrogen generation rate (mL $g^{-1}$ $min^{-1}$) | Volume of generated $H_2$ in 6 min (mL $g^{-1}$) | Total hydrogen generation volume in 1 h (mL $g^{-1}$) |
|---|---|---|---|---|---|
| Al | Li | Sn | | | |
| 84 | 0 | 16 | 105 | 540 | 920 (Ref. [22]) |
| 84 | 2 | 14 | 746 | 670 | 1000 |
| 84 | 4 | 12 | 846 | 805 | 1029 |
| 84 | 6 | 10 | 1057 | 904 | 1058 |
| 84 | 8 | 8 | 1137 | 982 | 1147 |
| 84 | 10 | 6 | - | - | 1090 |
| 84 | 12 | 4 | - | - | 1070 |
| 84 | 16 | 0 | - | - | 1025 |

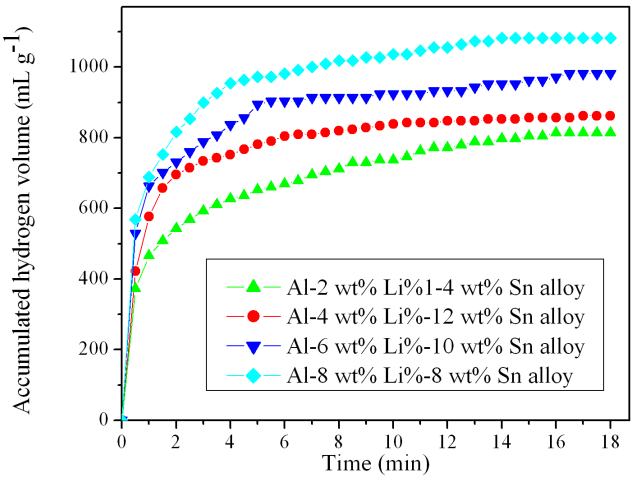


Figure 5. Hydrogen generation curves from the Al−8 wt% Li−8 wt% Sn alloy with a different Li/Sn ratio content.

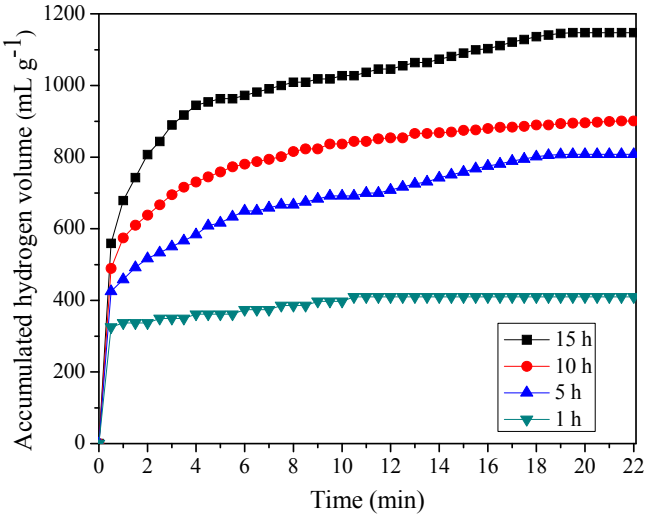


Figure 6. Hydrogen generation of the Al−8 wt% Li−8 wt% Sn alloy with a different milling time.

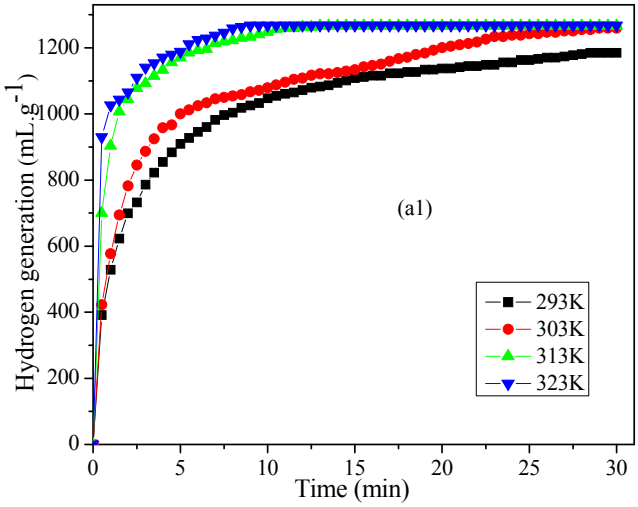


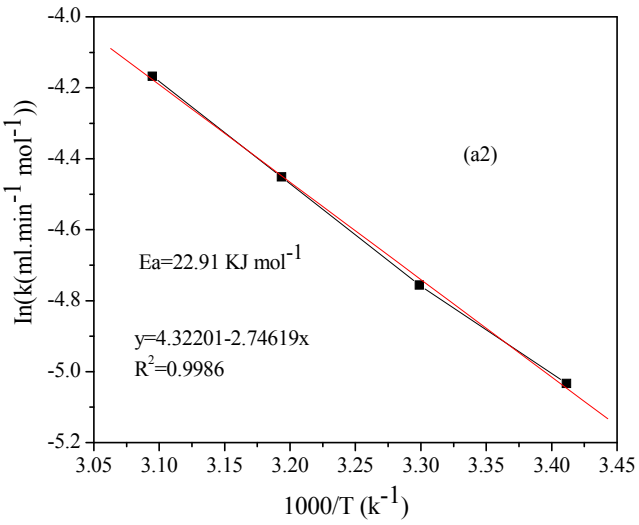


Figure 7. (a1) Hydrogen generation curves of the Al−8 wt% Li−8 wt% Sn alloy at different hydrolysis temperatures, (a2) the relationship of ln (K) and 1000/T.

tion rate and amount, are improved.

Fig. 5 shows the hydrogen generation curves from aluminum alloys with different Li/Sn weight ratios. Hydrogen generation curves undergo three stages: (1) the induction stage, (2) the high-hydrogen generation rate stage, and (3) the low-hydrogen generation-rate stage [10]. The induction stage depends on the additive type and grinding time, among others factors. This stage does not usually exceed 5 min and cannot be easily found in the hydrolysis process of aluminum mixtures with a long processing time and highly active additives. The hydrogen generation curves of aluminum alloys can rapidly transition into the second stage and have the largest hydrogen rate in the first 1 min of hydrolysis, as shown in Fig. 5. The high hydrogen generation rate at the initial point is due to the large exposure of water and the aluminum alloy. Most of the hydrogen gas is generated at the second stage, which lasts for about 5 min [14]. The duration of the first two stages of the hydrogen generation curves is proportional to the Li/Sn weight ratio.

The hydrogen generation characteristics of the Al−8 wt% Li−8 wt% Sn alloy prepared with different milling times are shown in Fig. 6. The accumulated hydrogen volume and hydrogen generation rate are largely dependent on the milling time. Most of the hydrogen volume is generated in the first 6 min of hydrolysis, and the value increases from 361 to 982 mL $g^{-1}$ when the milling time is prolonged from 1 to 15 h.

Meanwhile, the maximum hydrogen generation rate increases from 325 to 559 mL $g^{-1}$ $min^{-1}$. The improved hydrolysis properties that result from the longer milling times are attributed to several factors such as the larger surface area and the addition of new activated additives. The longer ball milling stimulates the formation of the Li−Sn alloy, decreases the alloy particle size, and makes Li/Sn uniformly distributed on the aluminum surface, as shown in Figs. 2 and 3. Many previous works [24] have also confirmed that compo-

nent redistribution, microstructure change, and grain size decrease result from a prolonged milling time.

The effect of the increase in global temperature from 293 to 323 K on the hydrogen generation rate of the 15 h-milled Al−8 wt% Li−8 wt% Sn alloy in pure water is shown in Fig. 7. As expected, the global temperature does not affects the hydrogen yield of the alloy in water, but and it improves its the hydrogen generation rate. The maximum hydrogen generation rate increases dramatically from 528 to 1,026 mL $g^{-1}$ $min^{-1}$ when the global temperature is increased from 293 to 323 K. To quantify this effect further, the Arrhenius equation is used:

$$k = A \cdot \exp\left(-E_a / RT\right) \tag{6}$$

where k is the reaction rate constant ($s^{-1}$), A indicates the constant pre-exponential factor ($s^{-1}$), R is the ideal gas constant (8.314 J $mol^{-1}$ $K^{-1}$), T is the temperature (K), and Ea is the activation energy (KJ $mol^{-1}$). k is commonly used as the maximum hydrogen generation rate in Fig. 7(a1). As shown in Reaction (6), the apparent activation energy associated with the hydrolysis reaction is controlled by a linear regression of ln (k) versus 1000/T. From Fig. 7(a2), a good fitting is obtained, and the apparent activation energy is determined to be 22.91 kJ $mol^{-1}$.

## 4. CONCLUSIONS

A hydrogen generation method using milled Al−Li−Sn alloy in water, which has good hydrogen yield and hydrogen generation rate, has been reported. A maximum hydrogen generation rate and amount of up to 1,137 mL $g^{-1}$ $min^{-1}$ and 1147 mL $g^{-1}$ , respectively, with 99% efficiency is obtained using Al−8 wt% Li−8 wt% Sn alloy in water. The enhanced hydrolysis properties of the aluminum alloy are mostly attributed to the presence of new $Li_xSn_y$ alloy phases (LiSn, $Li_5Sn_2$, and $Li_{13}Sn_5$), whereas the evolution from Sn to LiSn, $Li_5Sn_2$, and $Li_{13}Sn_5$ is obtained with an increase in Li/Sn weight ratio from 1:7 to 3:1. These compounds acts as hydrolysis centers and stimulate aluminum corrosion via the synergistic catalytic effect of Li and Sn metals. The hypothesis is further confirmed by the mechanism of aluminum alloy corrosion in water. The Li−Sn alloy with that haswith -2.906 V of standard potential, which is much lower than the -1.29 V potential of water decomposition potential, initially reacts with water to produce LiOH and Sn, which presentindicating its a highgood capability to accelerate aluminum corrosion. which show good abilitity to improve electrochemical corrosion of aluminum. Finally, the effects of global temperature and milling time have also been reported and explained.

## 5. ACKNOWLEDGMENT

This work was financially supported by the National Natural Science Foundation of China (Project Nos. 21003112 and 21003111), the Zhejiang Basic Research Program of China (Y4090507), and the Zhejiang Analysis Test Project of China (2009F70010).

## REFERENCES

[1] G.N. Marba, T.S. Valde, Int. J. Hydrogen Energy, 32, 1625 (2007).
[2] M. Balat, Int. J. Hydrogen Energy, 33, 4013 (2008).
[3] B. Wang, J. Power Sources, 152, 1 (2005).
[4] U.B. Demirci, O. Akdim, P. Miele, Int. J. Hydrogen Energy, 34, 2638 (2009).
[5] E. Fakiolu, Y. Yurum, T.N. Veziroglu, Int. J. Hydrogen Energy, 29, 1371 (2004).
[6] Y. Huang, Y. Wang, R. Zhao, P.K. Shen, Z. Wei, Int. J. Hydrogen Energy, 33, 7110 (2008).
[7] H. Lee, J.W. Lee, D.Y. Kim, J. Park, Y.T. Seo, H. Zeng, I.L. Moudrakovski, C.I. Ratcliffe, J.A. Ripmeester, Nature, 434, 743 (2005).
[8] M. Dornheim, N. Eigen, G. Barkhordarian, T. Klassen, R. Bormann, Advanced Engineering Materials, 8, 377 (2006).
[9] O.V. Kravchenko, K.N. Semenenko, B.M. Bulychev, K.B. Kalmykov, J. Alloys Compounds, 397, 58 (2005).
[10] E. Czech, T. Troczynski, Int. J. Hydrogen Energy, 35, 1029 (2010).
[11] A. Babak, M. Korosh, Int. J. Hydrogen Energy, 34, 7934 (2009).
[12] O. Noriyuki, Y. Takashi, Method of producing high-pressure containing gas for use as a power source, US3985866.
[13] C. Haertling, R.J. Hanrahan, J. Smith, R. Smith, J. Nuclear Materials, 309, 195 (2006).
[14] M.H. Grosjean, M. Zidoune, J.Y. Huot, Int. J. Hydrogen Energy, 31, 109 (2006).
[15] A.R. Shashikala, R. Umarani, S.M. Mayanna, A.K. Sharma, Int. J. Electrochem. Science, 3, 993 (2008).
[16] M.Q, Fan, F. Xu, L.X. Sun, Int. J. Hydrogen Energy, 32, 2809 (2007).
[17] http://www.physchem.co.za/Data/Electrode%20Potentials.htm
[18] S.I. Pyun, S.M. Moon, J. Solid State Electrochemistry, 4, 267 (2000).
[19] S. Tanaka, N. Hirose, T. Tanaki, Int. J. Hydrogen Energy, 25, 481 (2000).
[20] K.C. Emregul, A.A. Aksut, Corrosion Science, 42, 2051 (2000).
[21] A.R. Despic, J. Radosevic, P. Dabic, M. Kliskic, Electrochimica Acta, 35, 1743 (1990).
[22] H.B. Shao, J.Q. Zhang, J.M. Wang, Acta Physico–Chimica Sinica, 19, 372 (2003).
[23] M.Q. Fan, Y.Y. Liu, L.N. Yang, C.X. Cao, L.X. Sun, F. Xu, Chemical J. of Chinese Universities, 29, 356 (2008).
[24] C. Suryanarayama, Progress in Materials Science, 46, 1 (2001).